Performance Assessment: Influence of Sorbate-Sorbent Interphase Using Magnetite Modified Graphene Oxide to Improve Wastewater Treatment

Olayinka Oluwaseun Oluwasina[1,2], Mochamad Zakki Fahmi[1*], and Olugbenga Oludayo Oluwasina[3]

[1]*Department of Chemistry, Universitas Airlangga, Kampus C Mulyorejo, Surabaya 60115, Indonesia*

[2]*Department of Marine Science and Technology, The Federal University of Technology, P.M.B 704, Akure 340110, Nigeria*

[3]*Department of Chemistry, The Federal University of Technology, P.M.B 704, Akure 340110, Nigeria*

Corresponding author:

email: m.zakki.fahmi@fst.unair.ac.id

Received: February 20, 2023
Accepted: May 20, 2023

DOI: 10.22146/ijc.82454

Abstract: *The adsorption of brilliant green onto magnetite-graphene oxide nanoparticles (MGONPs) from an aqueous solution was explored via batch experiments. The adsorption properties of MGONPs were carried out under various experimental conditions related to pH, contact time, adsorbent dose, temperature, and initial adsorbate concentration. The adsorption capacity of MGONPs and optimum pH were 54.57 mg g^{-1} and 6, respectively. Equilibrium was attained after 30 min, and the adsorption kinetics data best fitted the pseudo-second-order. The Freundlich isotherm best fits the equilibrium. Acetone was able to desorb the dye from the loaded adsorbent. Additionally, the newly developed adsorption attributes effective surface area (eS_{BET}) and dimensionless preferential adsorption (q_p) were more accurate than the conventional specific surface area (S_{BET}). The adsorption capacity provides information about the sorbate-sorbent interface (q). The relevance and accuracy of the new parameters for future adsorption system design by correlation analysis were validated. This study confirms the successful modification of MGONPs for the sorption of the cationic dye brilliant green.*

Keywords: *magnetite-graphene oxide nanoparticles; preferential adsorption; specific surface area; effective surface area; brilliant green*

■ INTRODUCTION

The use and discharge of dye in waterbody have created toxicity risks for humans and aquatic creatures. The dye's color prevents sunlight penetration into the water body, resulting in a loss of primary productivity. Dye molecules can be classed based on their ionic charge, which can be zwitterionic, anionic, non-ionic, or cationic [1]. It has been reported over the years that there are more than 100,000 different synthetic dyes that are commercially available, with a yearly production of more than 700,000 metric tons [2]. It was revealed that about half of the applied dye was present in the effluent after analyzing the chemical composition of textile dye effluents. The high concentration of colors in wastewater from textile manufacturing has been connected to the low absorption properties of fibers of dyes [1]. The complex molecules that make up synthetic dyes are typically composed of azo, triphenylmethane, or heterocyclic/polymeric structures, and due to their stability, they can last for a very long time in the natural ecosystem without changing or being discolored. The excessive use of these dyestuffs has become a growing source of environmental concern. During production and use, more than 10 to 15% of dyes are released into the environment [3]. A million tons of azo dyes are estimated to be produced annually on a global scale. For a healthy ecology, a sustainable economy, and excellent health, there must be access to high-quality water. Lack of access to clean water is a severe issue in both industrialized and developing nations. Water that contains trace levels of color (less than 1 mg/L) is visibly unpleasant and inappropriate for irrigation, domestic use, or human eating [4].

Brilliant green (BG) is a cationic triaryl methane dye that comes in a yellowish-green powder. Because its

color change from green to yellow at pH 2, BG can also be used as an indicator, a biological stain in veterinary medicine, and a stabilizer in poultry feed to limit fungi attacks [5-6]. Exposure to this dye may cause gastrointestinal and respiratory tract issues and systemic dermatitis in humans, resulting in nausea, vomiting, diarrhea, cough, trouble breathing, and jaundice [7]. In addition, BG is toxic to aquatic life with long-term consequences. Brilliant green has been used as an antiseptic on the skin, but it is harmful when it comes into contact with the eyes.

Sedimentation, filtration, oxidation, electrochemical techniques, adsorption, and ion exchange have all been employed to remove dye from aqueous solutions [8-9]. Among the different methods utilized, adsorption has several advantages, including simplicity, high adsorption capacity, low cost, and environmental friendliness [10]. The use of nanoparticles for dye removal from wastewater has been investigated by various researchers [11-13]. Magnetite nanoparticles have recently received a lot of interest because they are inexpensive, environmentally acceptable, and easy to produce. These particles also exhibit excellent optical, chemical, and electrical properties and significant superparamagnetic capabilities. However, these particles agglomerate easily and oxidize quickly [14]. The aqueous dispersion of iron nanoparticles is improved by embedding them on sheets of carbonaceous materials, and graphene-based materials are kind of promising carbonaceous substances for such purposes [15].

Graphene oxide (GO)-based nanomaterial synthesized with iron nanoparticles exhibited improved dispersion behavior in water [16]. When graphite is oxidized, oxygen functional groups are introduced into the structure, making it hydrophilic and allowing it to form a stable suspension in aqueous conditions. GO is made by sonicating graphite oxide in water to exfoliate it. The high surface area of GO enables the incorporation of a wide range of functionalization groups into the sheets [17-18]. Graphene-based composites are formed by incorporating various functional groups, thereby improving the materials' photocatalytic, biocidal, electroactive, and capability [19-21]. Chemical modification of graphene-based materials has been used to develop nanocomposites with improved dispersion and compatibility in aqueous conditions. The integration of magnetite with graphene or GO may be a promising method for the removal of pollutants. Synthesis of magnetite-GO has recently been produced and utilized for drug delivery [22], magnetic-based imaging [23], and pollutant treatment from wastewater [24-27]. Magnetite-GO was synthesized for pollutant removal because of its stability and performance high.

However, there is no integrative report on the adsorption efficiency of brilliant green upon nanocomposite of magnetite-GO. Thus, in the present research, we focused on studying the design of magnetite-based nanocomposite material that can effectively remove emerging contaminants even when they are present in low concentrations (Scheme 1). The adsorption properties were examined by studying the effect of pH, the adsorption kinetics, and the adsorption isotherms to identify the adsorption mechanism. The study gives a novel assessment of the adsorbents' performance by computation of newly developed physical features, which shed light on the effect of the sorbents' physical and chemical properties and sorbates on the separation process. As a result, the statistical estimations used to assess the sorbents' efficiency are also presented. The interaction between the sorbent and sorbate is also carefully considered in relation to the contaminant's sorption.

■ EXPERIMENTAL SECTION

Materials

Chemicals such as graphite powder (20 μm, synthetic), sulfuric acid (98%, H_2SO_4), hydrochloric acid (30%, HCl), hydrogen peroxide (30%, H_2O_2), potassium permanganate ($KMnO_4$), ferrous ammonium sulfate, ammonium ferric sulfate, aqueous ammonia, sodium hydroxide pellets and brilliant green (BG, $C_{27}H_{33}N_2{\cdot}HO_4S$) were purchased from Sigma-Aldrich and used without further purification.

Instrumentation

UV-Visible absorption spectra of the sample obtained by UV-Vis-NIR spectrophotometer UV-3600 (Shimadzu, Japan). The morphology of MGONPs was determined by Ultra PLUS Field Emission Scanning Electron Microscopy instrument (Zeiss, Germany), and functional group data of the nanomaterial provided by Fourier transform infrared spectrometry Spectrum 100 spectrometer (PerkinElmer, USA). The textural properties, surface area and porosity of the material were measured with a Tristar II 3020 analyzer (Micromeritics, USA).

Procedure

Synthesis of graphene oxide

The synthesis of modified GO was prepared using the method reported by Oluwasina et al. [28]. About 4 g of graphite, 2 g of sodium nitrate, and 92 mL of concentrated H_2SO_4 were mixed with magnetic stirring in an ice bath to give a black slurry. $KMnO_4$ (12 g) was added slowly to keep the temperature below 5 °C. The suspension was removed from the ice bath and heated to 35–40 °C for 90 min. A 190 mL of deionized water was then added, and the temperature was adjusted to 98 °C for 20 min. A 40 mL of 30% H_2O_2 was added to the mixture (the mixture turned bright yellow). The mixture was diluted with 200 mL of deionized water and stirred for 30 min. The reaction product was centrifuged and washed with Milli-Q water and 10% HCl solution until the pH was neutral. The product was vacuum dried at 60 °C for 48 h and stored for further characterization and application.

Synthesis of magnetite-graphene oxide nanoparticles

Magnetite-graphene oxide nanoparticles (MGONPs) were prepared by co-precipitating iron oxide magnetic nanoparticles decorated on GO. Briefly, GO (1 g) was dispersed in deionized water (100 mL) and sonicated. Next, about 10.7 g ammonium ferric sulfate and 58 g ferrous ammonium sulfate were dissolved in 100 mL of deionized water under oxygen-free conditions. After that, 10 mL aqueous ammonia was added into the solution to give iron oxide nanoparticles, with the addition of GO. The reaction was stirred for 45 min at 85 °C and cooled at room temperature. The resulting MGONPs were collected by a magnet and washed with water and anhydrous ethanol, dried at 70 °C for 12 h in a vacuum oven.

Adsorption study

To obtain the concentrations required, working solutions of BG were produced from the stock solution, which is prepared by dissolution of BG (1 g) on deionized water (up to 1 mg dm^{-3}). Batch adsorption was performed by agitating 25 cm^3 of BG solutions of known concentration at a given temperature with a sorbent dosage of 10 mg, and the pH was changed by

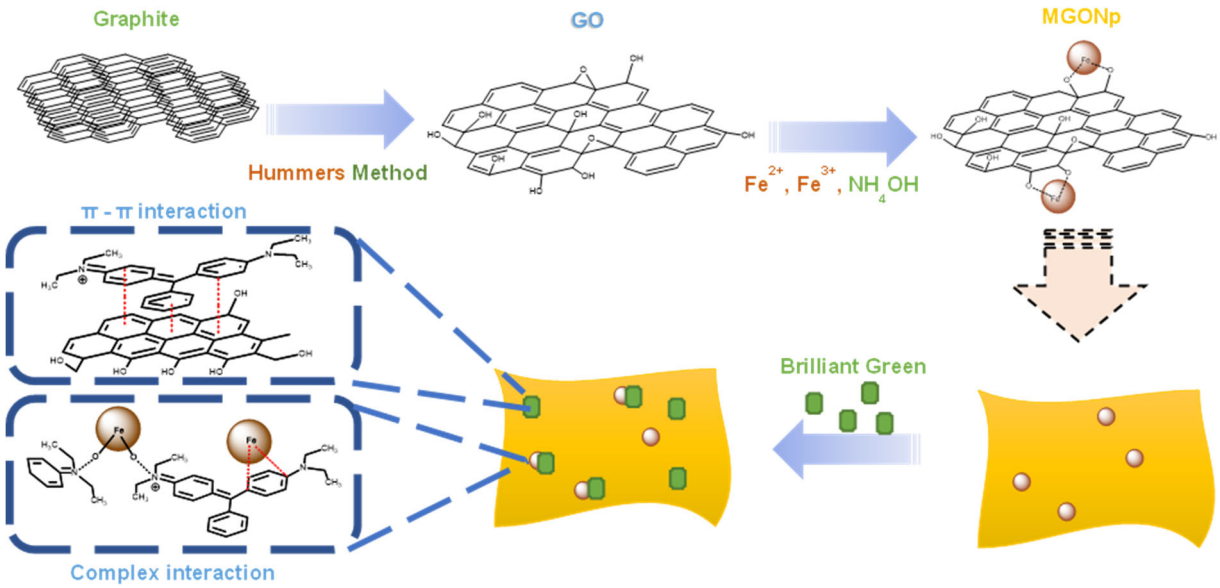

Scheme 1. Schematic illustration of MGONPs and the adsorption process of BG

Table 1. Adsorption isotherm models investigated for the sorption of BG onto MGONPs

Isotherm model	Equation*	Parameters	Reference
Langmuir	$q_{eq} = \frac{q_m b C_{eq}}{1 + b C_{eq}}$	q_m, b	[29]
Freundlich	$q_{eq} = K_F C_{eq}^{1/n}$	K_F, n	[30]
Sips	$q_{eq} = \frac{q_m b C_{eq}^{1/n}}{1 + b C_{eq}^{1/n}}$	q_m, b, n	[31]
Temkin	$q_{eq} = \frac{RT}{b_T} \ln(A_T C_{eq})$	b_T, A_T	[32]
Dubinin-Radushkevich	$\varepsilon = RT \ln\left(1 + \frac{1}{C_{eq}}\right)$	q_m, β	[33]
Redlich-Peterson	$q_{eq} = \frac{K_{RP} C_{eq}}{1 + a_{RP} C_{eq}^{g}}$	K_{RP}, a_{RP}, g	[34]
Khan	$q_{eq} = \frac{q_m b_K C_{eq}}{(1 + b_K C_{eq})^{a_K}}$	q_m, a_k, b_k	[35]

*q_{eq} is the adsorption capacity (mg g^{-1}); C_{eq} is the adsorbate equilibrium concentration in solution (mg dm^{-3}); q_m is the maximum monolayer capacity (mg g^{-1}); b is the Langmuir isotherm constant (dm^3 mg^{-1}); K_F is the Freundlich isotherm constant (mg g^{-1})(dm^3 mg^{-1}); n is the intensity of adsorption intensity; A_T, Temkin isotherm equilibrium binding constant (dm^3 g^{-1}); b_T, Temkin isotherm constant; β, Dubinin-Radushkevich isotherm constant (mol^2 kJ^{-2}); K_T, Redlich-Peterson isotherm constant (dm^3 g^{-1}); g, Redlich-Peterson isotherm exponent; a_{RP}, Redlich-Peterson isotherm constant; a_k, Khan isotherm exponent; b_k, Khan isotherm constant

adding either 0.1 M NaOH or HCl. The final concentration of the dye after filtering was determined at 624 nm by ultraviolet-visible (UV-Vis) spectrophotometry. The effects of pH, adsorbent dosage, temperature, and initial BG concentrations were investigated to identify the best adsorption conditions. The adsorption capacity was calculated by the Freundlich, Langmuir, and Sips models, respectively, presented in Table 1.

Eq. (1) and (2) were used to calculate the adsorption capacity (q_e) and efficiency, respectively.

$$(\%)\text{adsorbed} = \left(\frac{C_i - C_{eq}}{C_i}\right) \times 100\% \quad (1)$$

$$q_{eq} = \frac{V}{m} \times \left(C_i - C_{eq}\right) \quad (2)$$

where C_i represents the initial adsorbate concentration (mg dm^{-3}), q_e is the adsorption capacity (mg g^{-1}), C_{eq} is the equilibrium concentration of adsorbate (mg dm^{-3}), V is the adsorbate volume (dm^3), and m is the mass of adsorbent (mg).

Adsorption isotherms

The adsorption isotherms were investigated with BG concentrations ranging from 10 to 100 mg dm^{-3}. Aliquots of 25 cm^3 of varied concentration were introduced to 40 mg of adsorbents and shaken for 4 h in a thermostated shaking water bath at 298 K. The equilibrium concentration of BG in the suspensions was determined using UV-Vis spectrophotometry after 4 h. To analyze the equilibrium data, the isotherm models in Table 1 were used.

Adsorption kinetics

Adsorption kinetics was investigated by mixing a 25 cm^3 aliquot of a 20 mg dm^{-3} BG solution with a 40 mg adsorbent dosage. The time intervals for contacting the solutions were in the range of 5–300 min. UV-Vis spectrophotometry was used to determine the final concentration of BG after filtering. The experimental adsorption data attained through the batch studies were applied to the pseudo-first-order, pseudo-second-order, Elovich kinetics, and intraparticle diffusion models given in Table 2.

Desorption experiment

The desorption experiment was carried out by mixing 30 mg of the adsorbent with 25 cm^3 aliquots of 20 mg dm^{-3} BG solution for 3 h. After that, the mixture was filtered through a Whatman No. 1 filter paper, and

Table 2. Adsorption kinetics model explored for the removal of BG onto MGONPs

Kinetic model	Equation*	Parameters	Reference
Pseudo-first-order	$q_t = q_{eq}(1 - e^{-k_1 t})$	q_{eq}, k_1	[36-38]
Pseudo-second-order	$q_t = \frac{k_2 q_{eq}^2 t}{1 + k_2 q_{eq} t}$	k_2, q_{eq}	[36-37]
Intraparticle diffusion	$q_t = k_{id}(t)^{1/2} + c$	k_{id}, c	[39]
Elovich	$q_t = \frac{1}{\beta}\ln(1 + \alpha\beta t)$	α, β	[40]

*q_{eq} is the amount adsorbed at equilibrium (mg g^{-1}), q_t is the amount adsorbed at adjusted times (mg g^{-1}), k_1 is the pseudo-first-order rate constant (min^{-1}), k_2 is the pseudo-second-order rate constant (g mg^{-1} min^{-1}), k_{id} is the intraparticle diffusion rate constant (mg g^{-1} $min^{0.5}$), β is the Elovich parameter defined as the desorption constant (g mg^{-1}), α is the Elovich parameter defined as the initial adsorption rate (mg g^{-1} min^{-1})

the filtrate was analyzed for BG. The adsorbent that was filtered off was dried at 60 °C. After that, 20 mg of the BG loaded-adsorbent was added to a 25 cm^3 acetone and shaken for 12 h. The filtrate was analyzed using UV-Vis spectrophotometry after the mixture was filtered. SEM-EDX and FTIR were used to examine the loaded and desorbed adsorbent to evaluate if the dye had desorbed from the adsorbent surface. There was a significant change as the dye was desorbed on the surface of the adsorbent.

Data analysis

Using routine nls in the R statistical computing environment, the adsorption data were fitted into the adsorption isotherms and kinetics models. The model's effectiveness was determined by looking at the sum of squared residuals (SSR) and residual squared errors (RSE). The SSR of the model with the lowest SSR was chosen.

■ RESULTS AND DISCUSSION

Characterization of the Synthesized Material

The textural features of MGONPs were determined using N_2 adsorption-desorption isotherms. This provides information on the sample's pore volume size distribution and specific surface area. The pore volume determined according to nitrogen adsorption by the specified method applies only to mesopores and does not consider macropores (> 50 nm). Therefore, the pores could be grouped into micropores (< 2 nm), mesopores (2–50 nm), and macropores (> 50 nm). The result indicates that MGONPs are mesoporous, having an average pore diameter of 14.13 nm. The pore volume determined according to nitrogen adsorption by the specified method applies only to mesopores and does not take into account macropores (> 50 nm). In addition, the adsorbents exhibited type IV isotherms and

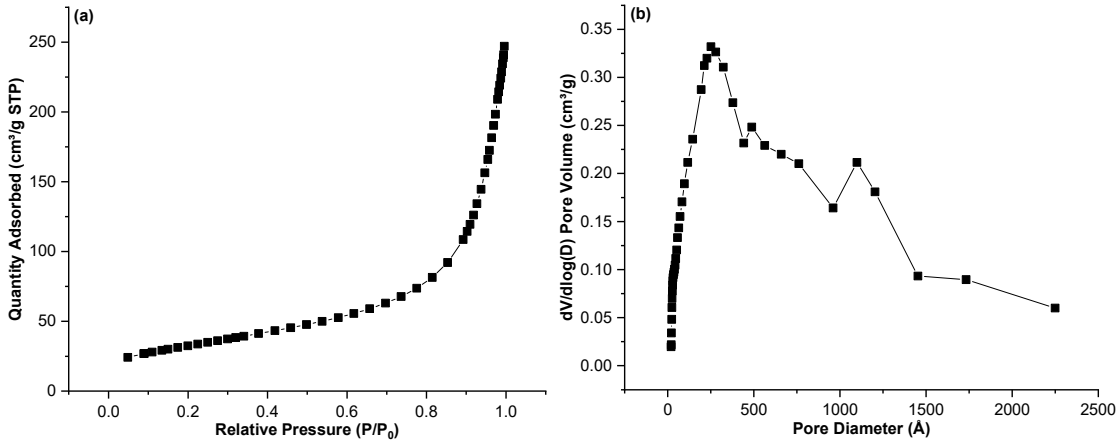

Fig 1. (a) BET Nitrogen adsorption-desorption isotherms and (b) BHJ pore volumes of MGONPs

H3-Type hysteresis loops, indicating that the nanomaterial is mesoporous [41]. Type IV represents an adsorption isotherm with hysteresis related to capillary condensation in mesopores. MGONPs showed a large surface area of 116.81 $m^2 g^{-1}$, having a Barrett–Halenda–Joyner (BHJ) based pore volume of 0.3763 $cm^3 g^{-1}$ (Fig. 1).

The FTIR spectrum displayed in Fig. 2 appears the functional groups on the surface of MGONPs. The absorption peak at around 598 cm^{-1} can be referred to as the Fe–O vibrational mode of Fe_3O_4 nanoparticles. The absorption peaks at 3604 and 1692 cm^{-1} correspond to the extending vibration of –OH and –FeOO, respectively [42]. This finding demonstrates that Fe_3O_4 successfully decorated the GO surface, as confirmed by SEM examination. In addition, the FTIR spectrum shows three broad peaks at 1749, 1565, and 1031 cm^{-1}, which correspond to the aromatic C=O stretch, C=C, and C-H stretching, respectively [43]. The peaks around 1938, 2091, and 2331 cm^{-1} correspond to the peaks of the dye molecules on the adsorbent.

The morphology of MGONPs was investigated using SEM, as shown in Fig. 3. The MGONPs have a

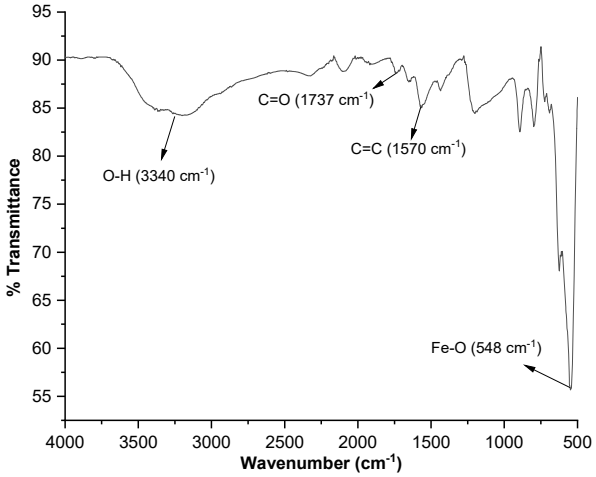

Fig 2. FTIR spectra of MGONPs before adsorption

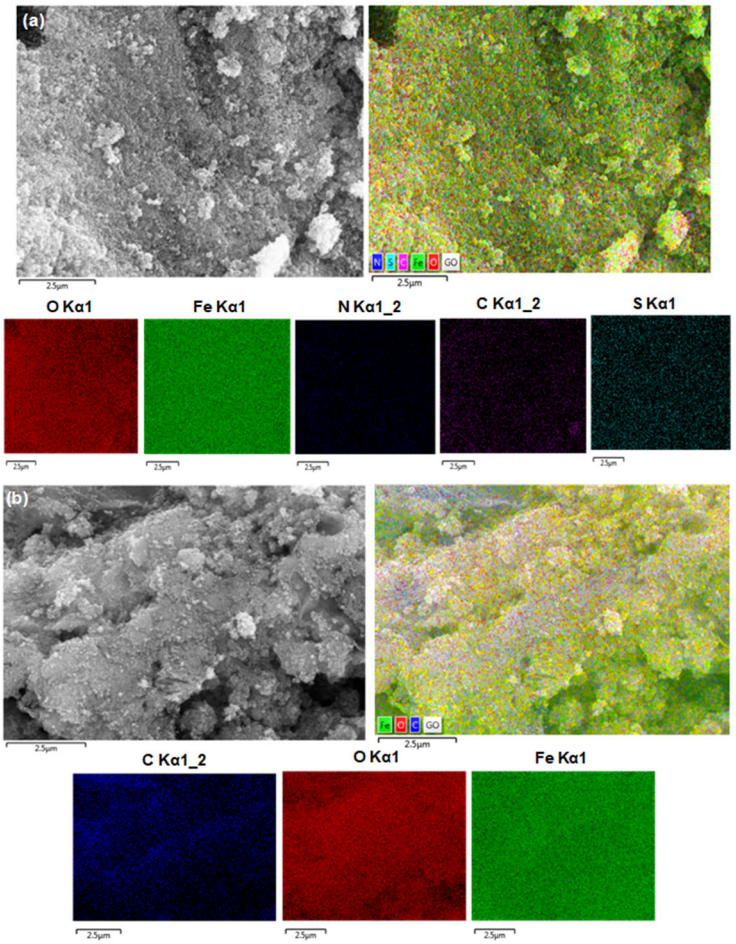

Fig 3. SEM and EDX images of MGONPs (a) after adsorption, 2.5 µm scale and (b) desorption of BG, 2.5 µm scale

crumpled surface. This might be the effect of the quick drying of the liquid phase from the MGONPs during the preparation process. Also, small granular particles were observed on its surface, where Fe_3O_4 deposits. The SEM-EDX images revealed that the dye molecules were adsorbed on the surface of the adsorbent during adsorption.

Sorption Characteristics

Batch adsorption tests for BG adsorption onto MGONPs were carried out to investigate the adsorbent's adsorption characteristics and efficiency in removing BG. pH, adsorbent dosage, contact time, temperature, and initial adsorbate concentration were all investigated as sorption parameters. The experimental data were also used to investigate adsorption isotherms and kinetics. Desorption tests for the dye were carried out to see if the adsorbents could be regenerated and reused.

Effect of pH

A solution's pH influences the dye structure and the adsorbent nature due to the ionization behavior and changes in surface charge, respectively [44]. The experiment pH was studied by varying the pH from 3 to 10 (using 0.1 g of adsorbent and 10 mg dm^{-3} BG concentration for 300 min contact time at 180 rpm) because at pH ≤ 2, the BG dye solution became colorless. The disparity of color concentration could result from its extended conjugated system of alternate double and single bonds. The reaction between OH^- ions and BG molecules occurs with conjugation interruption at higher pH values. The reduced color following increased pH may happen due to the central carbon atom of BG acting as an electrophilic center, and the OH^- is favored. The dye's rate of color change was faster in alkaline media, which could be attributed to its high nucleophilic nature. Decolorization of the dye could also occur through nucleophilic attack by H_3O^+, but the color fades more slowly in an acidic medium. A colorless compound is formed at low pH because H_3O^+ destroys the conjugation between the aromatic rings [45]. Fig. 4 depicts the outcome. The removal of BG was increased by increasing the pH to a maximum pH of 6 (46%) and then decreased to reach a minimum removal percentage at pH 9 (41%). It

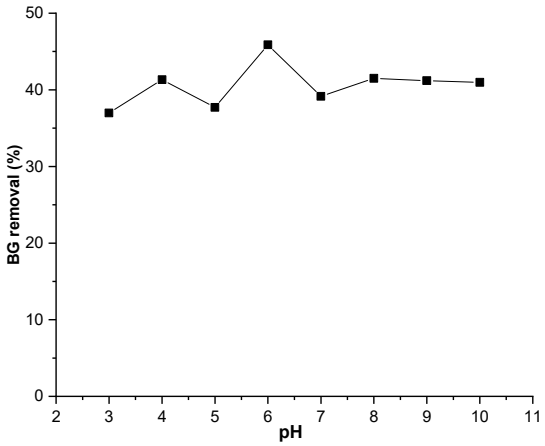

Fig 4. Effect of pH on the adsorption of BG (conditions: 25 cm^3 of 10 mg dm^{-3} BG, 5 h equilibration time, 10 mg sorbent dose, agitation speed of 180 rpm, temperature 298 K)

was discovered that the removal percentage in acidic environments is lower than in neutral environments. This could be due to the partial dissociation of surface functional groups in an acidic BG solution, resulting in electrostatic repulsion between the BG and MGONPs [46]. The reduction in the alkaline environments related to the neutral and acidic environment could be attributed to the higher electrostatic repulsion between the MGONPs and the dye molecules [47].

Given the structures of graphene's sp^2-bonded carbon particle, it is anticipated that a π–π interaction may play a critical part in the adsorption of natural fragrant compounds on MGONPs. There are a parcel more oxygen-containing useful bunches on the surface of MGONPs, and these bunches can work as electron-withdrawing bunches, localizing electrons from the π framework of graphene and interferometer with the π–π scattering strengths between the fragrant ring and graphene. The oxygen-containing functional groups repressed the adsorption of natural chemicals on carbon materials by means of water adsorption, dispersive-repulsive intelligence, and hydrogen holding, in this way driving the lower adsorption capacity of MGONPs [46].

Effect of dosage

By varying the mass of MGONPs from 10 to 120 mg, the effect of dosage on BG removal from aqueous solution was examined (Fig. 5). The result showed that the

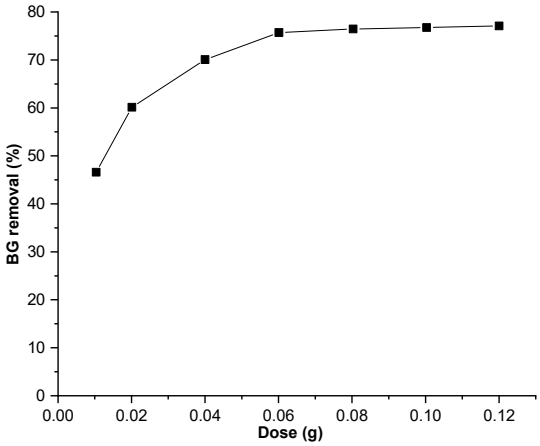

Fig 5. Effect of adsorbent dose on the sorption of BG (conditions: 25 cm^3 of 20 mg dm^{-3} BG, 4 h equilibration time, pH 6, agitation speed of 180 rpm, temperature 298 K)

percentage adsorbed increases as the adsorbent dose increases. For example, using 10 mg of MGONPs, a removal percentage of 46% was initially attained and then rose to 70% when the dosage was increased to 40 mg. After then, it increased to 75%, with no discernible increase in the percentage adsorbed. This could be because the nanocomposite agglomerated, reducing the surface area accessible for adsorption [48]. Furthermore, as the MGONPs dosage was increased from 10 to 40 mg, the BG percentage removal increased remarkably. This can be attributed to an increase in the number of unoccupied adsorption sites and functional groups on the adsorbent surface. This indicates that 40 mg has the necessary number of active sites to achieve maximal uptake.

Kinetics study

The removal of BG from MGONPs was investigated to establish the equilibrium sorption time, with time intervals ranging from 5 to 300 min. Fig. 6 shows the percentage of BG adsorbed onto the sorbent as a function of time. The percentage adsorbed onto MGONPs increases as the contact time increases, from the results obtained. After 30 min, the equilibrium was reached, with a maximum removal of 60%. After that, there was no discernible change in the BG concentration, indicating that the adsorption sites had been saturated [49].

The adsorption kinetics of BG using MGONPs were studied using four kinetics models: pseudo-first-order, pseudo-second-order, intraparticle diffusion, and Elovich models. The linear findings for the four kinetic models are shown in Fig. 7, and the kinetic parameters of the fitted models are listed in Table 3. Pseudo-second-order model better explained the adsorption of BG onto MGONPs. The experimental q_e values obtained are near the calculated values for both pseudo-first-order and pseudo-second-order models. The results of these models revealed that BG adsorption on MGONPs occurred via a biomolecular interaction involving the exchange or sharing of electrons between the adsorbent and the dye. As a result, the sorbent's adsorption capacity is related to its surface's number of active sites [51]. The following steps are involved in explaining the diffusion mechanism of adsorption processes: a) transfer

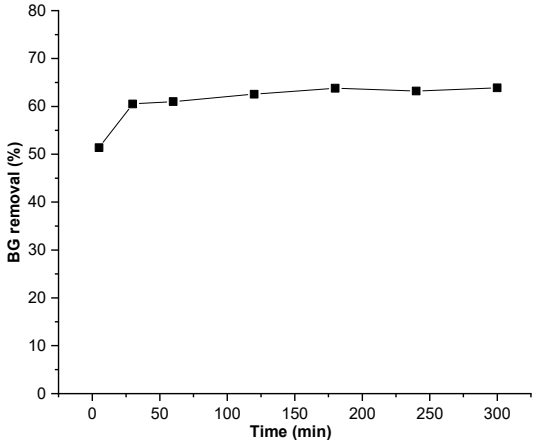

Fig 6. Effect of contact time on the sorption of BG (conditions: 25 cm^3 of 20 mg dm^{-3} BG, 40 mg sorbent dose, speed of 180 rpm, pH 6, temperature 298 K)

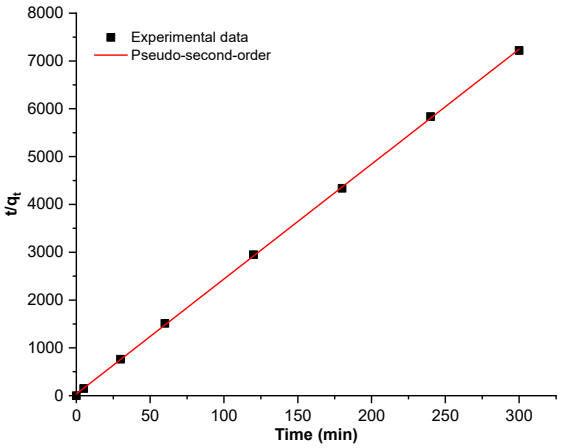

Fig 7. Pseudo-second-order kinetic model

Table 3. The calculated parameters for the four kinetics models tested for the sorption of BG onto MGONP**s** at different time intervals

Model	Parameters	BG
Experimental	q_{eq}/mg g^{-1}	0.053
Pseudo-first-order	$q_{eq.cal}$/mg g^{-1}	0.051
	$k_1/10^{-2}$/min	-0.001
	R^2	0.112
Pseudo-second-order	q_{eq}/mg g^{-1}	0.0410
	$k_2/10^{-3}$/g mg^{-1} min^{-1}	17.050
	R^2	0.999
Intraparticle diffusion	k_{id}/mg g^{-1} $min^{-0.5}$	0.002
	R^2	0.406
Elovich	α/mg g^{-1} min^{-1}	529.100
	β/g mg^{-1}	16.650
	R^2	0.887

Conditions: 25 cm^3 of 20 mg dm^{-3} BG, pH 6, 40 mg adsorbent, agitation speed 180 rpm, temperature 25 °C

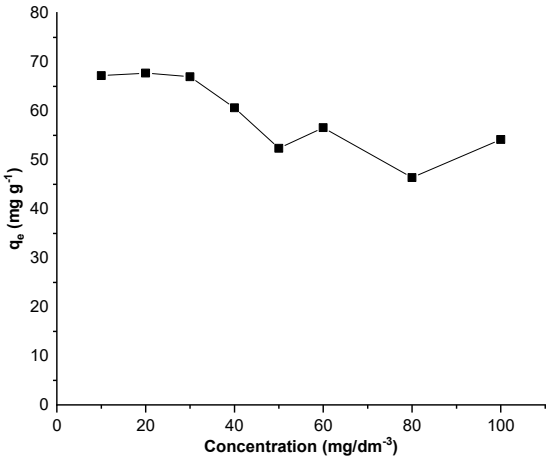

Fig 8. Effect of initial concentration on the adsorption of BG onto MGONPs (conditions: 25 cm^3 of 10 to 100 mg dm^{-3} BG solution, 40 mg adsorbent dose 4 h equilibration time, pH 6, agitation speed of 150 rpm, the temperature of 298 K)

of the adsorbate from the bulk solution to the surface of the solid phase; b) passage through the liquid film attached to the solid surface (film diffusion); c) internal mobility by pore dispersion from the surface of the solid phase to the inner surface of the permeable structure (intraparticle diffusion); and d) diffusion of the solute on the adsorption sites of the solid phase bringing about physisorption and chemisorption on the surface of the solid phase [52]. The intraparticle diffusion show was utilized to decide the rate-limiting step of the method. In the event that a direct plot that passes through the origin is gotten, adsorption is said to happen as it were by intraparticle diffusion [52]. It is presumed that two or more stages regulate the process if a linear plot that does not pass through the origin is obtained. The linear graphs obtained in this investigation passed through all the dots for pseudo-second-order, which indicates that the model is suitable for the experimental data.

Adsorption isotherms

Over a concentration range of 10 to 100 mg dm^{-3}, the influence of initial BG concentration on adsorption onto MGONPs was examined. As the dye concentration increased, the percentage of dye removed decreased (Fig. 8). This could be owing to the fixed number of active sites available for BG molecules on the adsorbent. At higher dye concentrations, the active sites of the adsorbent become saturated, and the adsorption capacity is thus determined by the initial concentration [50].

The equilibrium adsorption isotherm is required to determine the interacting behavior between the adsorbent and the adsorbent. It is also essential for the adsorption system's strategy. The Langmuir adsorption isotherm assumes that the binding sites are evenly distributed across the sorbent surface and have a similar affinity for single molecular layer sorption. The bonding to the sorption sites might be chemical or physical, but it must be sufficiently strong to prevent the adsorbed molecules from being displaced [53-54]. According to the Freundlich adsorption isotherm, sorption occurs on a heterogeneous surface, implying multilayer adsorption. This means that as the starting concentration of the solution is increased, the adsorbate concentration will rise [55-56]. The Langmuir and Freundlich models were used to fit the experimental equilibrium data. The slope and intercept of each equilibrium graph were used to calculate the Langmuir and Freundlich parameters (Fig. 9).

Table 4 appear the adsorption isotherm parameters for models that fitted the test balance information for BG adsorption. The Freundlich isotherm best fits the

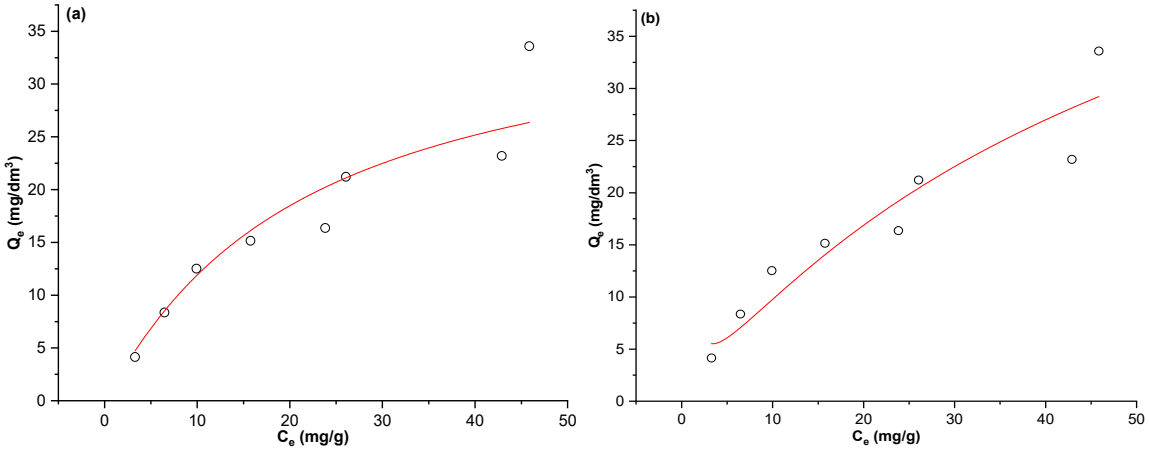

Fig 9. The Langmuir (a) and Freundlich (b) adsorption isotherms fitted the experimental data for the sorption of BG onto MGONPs

Table 4. Isotherm models' parameters

Isotherms	Parameters	Value
Freundlich	k_F/mg g^{-1}	2.412
	n	1.567
	SSR*	16.640
	RSE*	3.024
Langmuir	q_m/mg g^{-1}	54.572
	b/dm^3 mg^{-1}	0.024
	SSR	16.867
	RSE	3.228
Sips	q_m	5.932
	b	6.994
	n	1.606
	SSR	66.621
	RSE	5.176
Temkin	K	0.389
	b	282.010
	SSR	17.830
Dubinin-Radushkevich	q_m	25.220
	e	207.33
	SSR	28.690
Redlich-Peterson	K	0.3896
	a	0.0126
	g	1.7025
Klan	q_m	5.9320
	a	1.2607
	b	6.994
	SSR	586.24

*SSR: sum of squared residuals; *RSE: residual squared error

information based on the whole of SSR gotten. The Freundlich isotherm demonstration is based on the wonders of heterogeneous surfaces with a few adsorption components included, where K_F and n are the Freundlich constants related to the adsorption capacity and adsorption concentrated, respectively. The Freundlich parameter, n, shows the adsorption favorability. When the adsorption intensity, $n < 1$, it shows the favorability of the adsorption intensity over all the concentration ranges studied, but if $n > 1$, it shows that the adsorption intensity is favorable at high concentrations but less at lower concentrations [57]. The experimental data obtained for MGONPs shows an n value greater than 1, indicating that adsorption is favorable at higher concentrations but less at lower concentrations. According to the Langmuir model, q_m was 54.57 mg g^{-1}. On the other hand, the Freundlich model yielded an adsorption intensity value of 1.57, indicating a successful adsorption process [58].

The Langmuir adsorption capacities (q_m) of MGONPs were stacking up with various reported adsorbents for the removal of BG. Table 5 shows that the removal (q_m) by MGONPs used in this study compares favorably with other adsorbents.

The Langmuir model results in some parameters that can be used to estimate the favorability of the adsorption process. The separation factor (R_L), was calculated by using Eq. (3) [64]:

$$R_L = \frac{1}{1 + bC_i} \quad (1)$$

where C_i denotes the initial BG concentrations (mg dm^{-3}),

Table 5. Comparison of adsorption capacity of various reported adsorbents

Adsorbent	Temperature/K	q_m/mg g^{-1}	Reference
Hydroxyapatite/chitosan composite	-	49.10	[59]
Luffa cylindrical sponge	303	18.52	[60]
Corncob biochar	-	16.53	[61]
Areca nut husk	298	18.21	[62]
Poly(AN-coVP)/Zeolite composite	303	19.61	[63]
MGONPs	298	54.57	This study

and b denotes the Langmuir constant (dm^3 mg^{-1}). The value of R_L can be used to calculate the sequestration process's favorability. If $0 < R_L < 1$, adsorption is assumed to be favorable, unfavorable if $R_L > 1$, irreversible if $R_L = 0$, and linear if $R_L = 1$ [64]. All R_L values obtained in this study were found to fall between $0 < R_L < 1$; hence, the removal of BG onto MGONPs showed favorable adsorption. The procedure is more favorable when R_L values are minimal (Fig. 10).

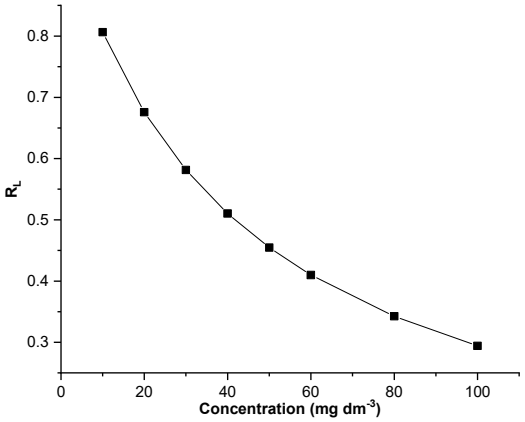

Fig 10. Separation factor R_L of BG onto MGONPs

Preferential adsorption

The special sorbate adsorption (q_p) and viable surface region (eS_{BET}) are the novel adsorption properties calculated for the performance evaluations. The found eS_{BET} is noteworthy since, notwithstanding the general S_{BET} of the adsorbent, chemical species adsorption pivots on the number of germane dynamic locales with a great fondness for the sorptive. The determination of eS_{BET} gives data on the importance of the dynamic locales to the q and, more essentially, the q_p esteem. Most of the considerations inspected within the current work did not allow data with respect to the sorts or sums of chemical functionalities on the sorbents. As a result, it is expected that the eS_{BET} will rise directly as long as the pertinent chemical surface usefulness is shown on the S_{BET}, either normally or misleadingly, through chemical impregnation. Table 6 appears the calculated adsorption parameters and highlights from the literature.

The adsorbent's mass adsorption capacity (q, mg g^{-1}) for a particular dye serves as the primary indicator for determining the extent of the sorbate-sorbent interphase. Only 2 of the 22 studies (Table 6) showed q_p values greater than 1, indicating that the sorbates preferred the sorbent to remain in the solution. The highest values were reported by Li et al. [76] (SN = 18; q_p = 49, ZnO nanoparticles on Congo red) and Lv et al. [77] (SN = 19; q_p = 336, sodium alginate/graphite based on malachite green), respectively. Fig. 11 shows a plot revealing the trend in the reported and derived adsorption properties for the selected adsorbents and pollutants.

The dataset's correlation data are shown in Table 7. After looking into the analyses, we found that the correlations increased noticeably. The q for brilliant green and the other adsorbates showed a similar trend with eS_{BET} (35.61 and 81.19%) than with S_{BET} (18.88 and 71.58%), respectively. The negative correlations between S_{BET} and eS_{BET} demonstrate that an adsorbent's adsorption capability is not always correlated with its S_{BET}. Inclusive, the derived adsorption properties (q_p and eS_{BET}) are much more consistent for equitable comparison between studies with various experimental settings and research goals.

The moles of the sorbent and q_p value of the adsorbate over solubility performed a positive relationship. Therefore, the more the sorbate's mass transfers onto the adsorbent, the higher the sorbent mass

Table 6. Estimated adsorption features of the various experiments

S/N	Dye	Sorbent mass (g)	q (mol g^{-1})	Surface area (m^2 g^{-1})	Effective Surf. Area (mol m^{-2})	Moles of sorbent (mol)	Volume (L)	Solubility (mol L^{-1})	Moles in solution (mol)	qp (Sorbent/Sol)	Ref
1	BG	0.01	4.75×10^{-4}	84.25	5.63×10^{-6}	4.75×10^{-6}	0.01	8.29×10^{-4}	8.29×10^{-4}	0.060	[65]
2	BG	0.01	3.11×10^{-4}	2.94	1.06×10^{-4}	3.11×10^{-6}	0.01	8.29×10^{-4}	8.29×10^{-4}	0.038	[65]
3	BG	0.01	1.71×10^{-3}	495.54	3.45×10^{-6}	1.71×10^{-5}	0.01	8.29×10^{-4}	8.29×10^{-4}	0.021	[65]
4	BG	0.80	1.86×10^{-4}	310	6.01×10^{-7}	1.49×10^{-4}	0.05	8.29×10^{-4}	4.14×10^{-3}	0.036	[66]
5	BG	1.00	3.43×10^{-5}	770.69	4.44×10^{-8}	3.43×10^{-5}	0.10	8.29×10^{-4}	8.29×10^{-3}	0.004	[61]
6	BG	1.20	1.15×10^{-3}	3.07	3.75×10^{-4}	1.38×10^{-3}	0.025	8.29×10^{-4}	2.07×10^{-3}	0.666	[67]
7	BG	0.04	4.93×10^{-4}	5.60	8.81×10^{-5}	1.97×10^{-5}	0.05	8.29×10^{-4}	4.14×10^{-3}	0.005	[68]
8	BG	0.005	2.03×10^{-6}	92	2.21×10^{-08}	1.01×10^{-8}	0.005	8.29×10^{-4}	4.14×10^{-3}	2.45×10^{-5}	[69]
9	BG	0.10	2.01×10^{-5}	19.64	1.02×10^{-6}	2.01×10^{-6}	0.05	8.29×10^{-4}	4.14×10^{-3}	4.85×10^{-4}	[63]
10	BG	0.03	3.48×10^{-4}	110	3.16×10^{-6}	1.04×10^{-5}	0.01	8.29×10^{-4}	8.29×10^{-4}	0.013	[70]
11	BG	0.75	2.30×10^{-4}	232.31	9.91×10^{-7}	1.73×10^{-4}	0.10	8.29×10^{-4}	8.29×10^{-3}	0.021	[71]
12	BG	0.40	2.59×10^{-4}	100.28	2.58×10^{-6}	1.03×10^{-4}	0.10	8.29×10^{-4}	8.29×10^{-3}	0.013	[72]
13	BG	0.10	5.93×10^{-4}	2304	2.57×10^{-7}	5.93×10^{-5}	0.05	8.29×10^{-4}	4.14×10^{-3}	0.014	[73]
14	BG	0.05	5.68×10^{-4}	1035	5.48×10^{-07}	2.84×10^{-5}	0.02	8.29×10^{-4}	1.66×10^{-3}	0.017	[74]
15	BG	0.05	6.96×10^{-4}	1425	4.88×10^{-7}	3.48×10^{-5}	0.02	8.29×10^{-4}	1.66×10^{-3}	0.021	[74]
16	BG	0.05	9.28×10^{-4}	424	2.19×10^{-6}	4.64×10^{-5}	0.01	8.29×10^{-4}	8.29×10^{-4}	0.056	[75]
17	BG	0.04	1.13×10^{-4}	116.81	9.68×10^{-7}	4.52×10^{-6}	0.025	8.29×10^{-4}	2.07×10^{-3}	0.002	This study
18	Congo red	0.04	1.02×10^{-4}	5.60	1.83×10^{-5}	4.09×10^{-6}	0.05	1.66×10^{-6}	8.32×10^{-8}	49.241	[76]
19	Malachite green	0.005	7.36×10^{-3}	237.42	3.10×10^{-5}	3.68×10^{-5}	0.01	1.10×10^{-5}	1.10×10^{-7}	335.945	[77]
20	Methylene blue	0.005	4.75×10^{-4}	85.60	5.55×10^{-6}	2.37×10^{-6}	0.01	0.14	1.36×10^{-3}	1.74×10^{-3}	[78]
21	Neutral red	0.005	1.06×10^{-3}	68.20	1.55×10^{-5}	5.30×10^{-6}	0.015	0.17	2.59×10^{-3}	2.04×10^{-3}	[79]
22	Methyl orange	0.15	8.53×10^{-5}	186	4.58×10^{-7}	1.27×10^{-5}	0.05	0.02	7.64×10^{-4}	1.67×10^{-2}	[80]

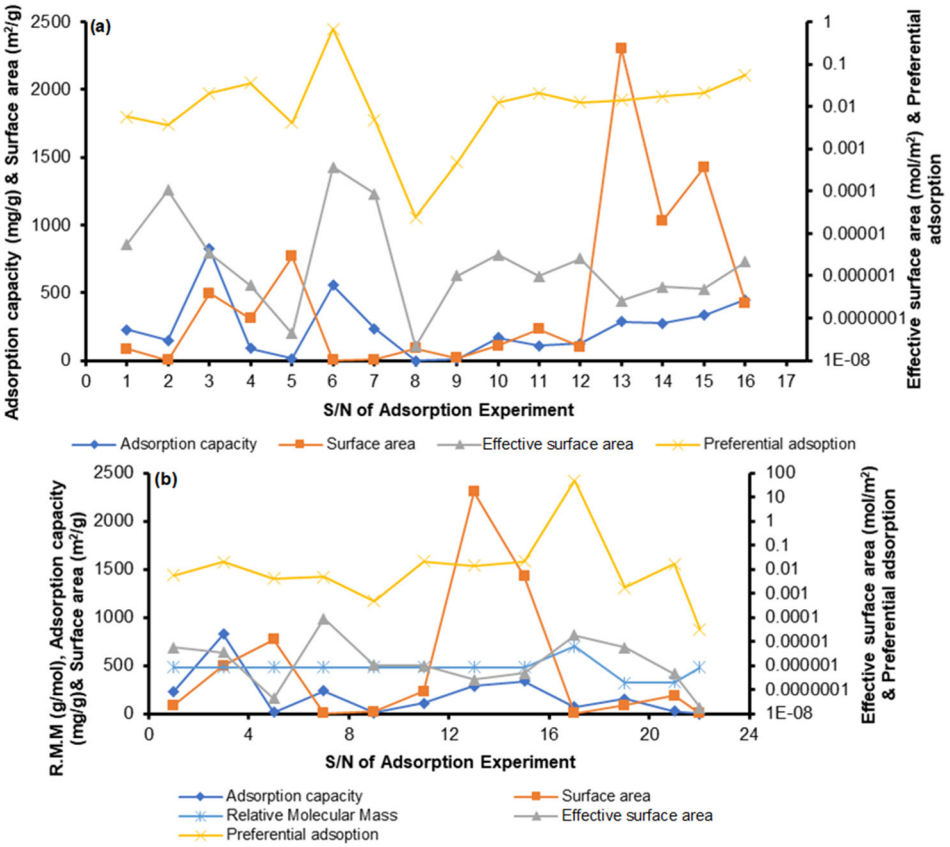

Fig 11. The several properties of (a) different adsorbents towards brilliant green, and (b) various adsorbents towards brilliant green and other dyes of different relative molecular mass, (S/N 1-16, and 17-22) in Table 6, respectively

Table 7. Correlation data of reported and derived adsorption properties of sorbate and sorbents

Adsorption properties	Sorbent mass vs. Moles in solution	q vs. S_{BET}	eS_{BET} vs. q_p	Moles of sorbent vs. q_p	S_{BET} vs. eS_{BET}	Sorbent mass vs. eS_{BET}	q vs. eS_{BET}
All	0.6088	0.0137	0.0037	-0.0506	-0.2188	0.5017	0.1037
Brilliant green	0.5795	0.1883	0.9283	0.9903	-0.2710	0.4955	0.3561
Others	-0.2262	0.7158	0.8315	0.9344	0.3736	-0.5728	0.8119

in the solution. For brilliant green (99%) and other dyes (93.45%), the relationship between the moles of sorbent and q_p is significant, demonstrating the agreement between the sorptive and the sorbents in this adsorption relationship [81-82].

■ CONCLUSION

This study revealed the successful modification of MGONPs for the adsorption of the cationic brilliant green dye from an aqueous solution. The following are the conclusions achieved from the study; the removal of BG was increased by increasing the pH to a maximum pH of 6, then decreased to reach a minimum removal percentage at pH 9. The pseudo-second-order model best described the experimental adsorption data fitted into the kinetic models. The adsorption isotherms study revealed that the Freundlich model best-fitted MGONPs. The maximum adsorption capacity (q_m) for MGONPs was 54.57 mg g^{-1}. A desorption study was carried out, and the SEM-EDX revealed that the dye molecules were desorbed after using acetone as the desorbing agent. The FTIR analysis showed the disappearance of the characteristic BG dye peaks after the desorption study. This showed that acetone is an excellent desorbing agent for BG, and the adsorbents can be recovered and recycled for reuse. Thus, this study indicates that MGONPs is a better adsorbent with higher adsorption capacity for the uptake of BG, and its application in the industry could be further explored. Additionally, dimensionless preferential adsorption (q_p) and effective surface area (eS_{BET}) performed more accurately than the conventional adsorption capacity and specific surface area (S_{BET}) in providing information about the sorbate-sorbent interface (q). We also validated the relevance and accuracy of the new parameters for future adsorption system design by correlation analysis. Adsorption is, therefore, an excellent method for reducing brilliant green pollutants in an aqueous medium.

■ ACKNOWLEDGMENTS

The authors thank the Universitas Airlangga Postdoctoral Fellowship, Indonesia, for the financial support of this work. This work was supported by the Universitas Airlangga Postdoctoral Fellowship, Indonesia (Ref No: 2480/UN3.22/KS/2022).

■ AUTHOR CONTRIBUTIONS

Olayinka Oluwaseun Oluwasina contributed in Conceptualization, Visualization, Investigation; Olayinka Oluwaseun Oluwasina contributed in Data curation, Writing- Original draft preparation; Mochamad Zakki Fahmi contributed in Supervision, Methodology, Writing- Reviewing and Editing.

■ REFERENCES

[1] Jadhav, I., Vasniwal, R., Shrivastava, D., and Jadhav, K., 2016, Microorganism-based treatment of azo dyes, *J. Environ. Sci. Technol.*, 9 (2), 188–197.

[2] Rani, B., Kumar, V., Singh, J., Bisht, S., Teotia, P., Sharma, S., and Kela, R., 2014, Bioremediation of dyes by fungi isolated from contaminated dye effluent sites for bio-usability, *Braz. J. Microbiol.*, 45 (3), 1055–1063.

[3] Alabdraba, W.M.S., and Albayati, M.B.A., 2014, Biodegradation of Azo Dyes—A Review, *Int. J. Environ. Sci. Nat. Resour.*, 4, 179–189.

[4] Zaman, A., Das, P., and Banerjee, P., 2016, "Biosorption of Dye Molecules" in *Toxicity and Waste Management Using Bioremediation*, Eds. Rathoure, A.K., and Dhatwalia, V.K., Global IGI, New York, US, 51–74.

[5] Vaid, V., and Jindal, R., 2022, An efficient pH-responsive kappa-carrageenan/tamarind kernel powder hydrogel for the removal of brilliant green and rose Bengal from aqueous solution, *J. Appl. Polym. Sci.*, 21, 139–151.

[6] Pandey, S., Do, J.Y., Kim, J., and Kang, M., 2020, Fast and highly efficient removal of dye from aqueous solution using natural locust bean gum based hydrogels as adsorbent, *Int. J. Biol. Macromol.*, 143, 60–75.

[7] Manickam, P., and Vijay, D., 2021, "Chemical Hazards in Textiles" in *Chemical Management in Textiles and Fashion*, Eds. Muthu, S.S., Woodhead Publishing, Cambridge, US, 19–52.

[8] Song, W., Li, J., Wang, Z., and Zhang, X., 2019, A mini review of activated methods to persulfate-based advanced oxidation process, *Water Sci. Technol.*, 79 (3), 573–579.

[9] Oguntimein, G., 2015, Biosorption of dye from textile wastewater effluent onto alkali treated dried sunflower seed hull and design of a batch adsorber, *J. Environ. Chem. Eng.*, 3 (4, Part A), 2647–2661.

[10] Chaari, I., Fakhfakh, E., Medhioub, M., and Jamoussi, F., 2019, Comparative study on adsorption of cationic and anionic dyes by smectite rich natural clays, *J. Mol. Struct.*, 1179, 672–677.

[11] Mahmoud, H.R., Ibrahim, S.M., and El-Molla, S.A., 2016, Textile dye removal from aqueous solutions using cheap MgO nanomaterials: Adsorption kinetics, isotherm studies and thermodynamics, *Adv. Powder Technol.*, 27 (1), 223–231.

[12] Fan, Y.H., Zhang, S.W., Qin, S.B., Li, X.S., and Qi, S.H., 2018, An enhanced adsorption of organic dyes onto NH_2 functionalization titanium-based metal-organic frameworks and the mechanism investigation, *Microporous Mesoporous Mater.*, 263, 120–127.

[13] Sirajudheen, P., Manuvel, R., Perumal, K., and Sankaran, M., 2020, Perceptive removal of toxic azo dyes from water using magnetic Fe_3O_4 reinforced graphene oxide–carboxymethyl cellulose recyclable composite: Adsorption investigation of parametric studies and their mechanisms, *Surf. Interfaces*, 21, 100648.

[14] Stefaniuk, M., Oleszczuk, P., and Ok, Y.S., 2016, Review on nano zerovalent iron (nZVI): From synthesis to environmental applications, *Chem. Eng. J.*, 287, 618–632.

[15] Mortazavian, S., An, H., Chun, D., and Moon, J., 2018, Activated carbon impregnated by zero-valent iron nanoparticles (AC/nZVI) optimized for simultaneous adsorption and reduction of aqueous hexavalent chromium: Material characterizations and kinetic studies, *Chem. Eng. J.*, 353, 781–795.

[16] Yoon, Y., Park, W.K., Hwang, T.M., Yoon, D.H., Yang, W.S., and Kang, J.W., 2016, Comparative evaluation of magnetite-graphene oxide and magnetite-reduced graphene oxide composite for As(III) and As(V) removal, *J. Hazard. Mater.*, 304, 196–204.

[17] Fahmi, M.Z., Wathoniyyah, M., Khasanah, M., Rahardjo, Y., and Wafiroh, S., 2018, Incorporation of graphene oxide in polyethersulfone mixed matrix membranes to enhance hemodialysis membrane performance, *RSC Adv.*, 8 (2), 931–937.

[18] Fahmi, M.Z., Andriyani, V., Dzikri, M.F., Armedya, T.P., Wathoniyyah, M., Wibowo, D.L.N., and Permana, A.J., 2019, *In situ* synthesis process of nanographene and its characteristic, *IOP Conf. Ser.: Earth Environ. Sci.*, 245, 012045.

[19] Kemp, K.C., Seema, H., Saleh, M., Le, N.H., Mahesh, K., Chandra, V., and Kim, K.S., 2013, Environmental applications using graphene composites: Water remediation and gas adsorption, *Nanoscale*, 5 (8), 3149–3171.

[20] Purnamasari, W., Budiastanti, T.A., Aminatun, A., Rahmah, U., Sumarsih, S., Chang, J.Y., and Fahmi, M.Z., 2022, Naproxen release behaviour from graphene oxide/cellulose acetate composite nanofibers, *RSC Adv.*, 12 (13), 8019–8029.

[21] Ramalingam, G., Perumal, N., Priya, A.K., and Rajendran, S., 2022, A review of graphene-based semiconductors for photocatalytic degradation of pollutants in wastewater, *Chemosphere*, 300, 134391.

[22] Fahmi, M.Z., Prasetya, R.A., Dzikri, M.F., Sakti, S.C.W., and Yuliarto, B., 2020, $MnFe_2O_4$ nanoparticles/cellulose acetate composite nanofiber for controllable release of naproxen, *Mater. Chem. Phys.*, 250, 123055.

[23] Torkashvand, N., and Sarlak, N., 2019, Synthesis of completely dispersed water soluble functionalized graphene/γ-Fe_2O_3 nanocomposite and its application as an MRI contrast agent, *J. Mol. Liq.*, 291, 111286.

[24] Liu, M., Chen, C., Hu, J., Wu, X., and Wang, X., 2011, Synthesis of magnetite/graphene oxide composite and application for cobalt(II) removal, *J. Phys. Chem. C*, 115 (51), 25234–25240.

[25] Weng, X., Lin, Z., Xiao, X., Li, C., and Chen, Z., 2018, One-step biosynthesis of hybrid reduced graphene oxide/iron-based nanoparticles by eucalyptus extract and its removal of dye, *J. Cleaner Prod.*, 203, 22–29.

[26] Rodríguez-García, S., Santiago, R., López-Díaz, D., Merchán, M.D., Velázquez, M.M., Fierro, J.L.G., and Palomar, J., 2019, Role of the structure of graphene oxide sheets on the CO_2 adsorption properties of nanocomposites based on graphene oxide and polyaniline or Fe_3O_4-nanoparticles, *ACS Sustainable Chem. Eng.*, 7 (14), 12464–12473.

[27] Kazemi, A., Bahramifar, N., Heydari, A., and Olsen, S.I., 2019, Synthesis and sustainable assessment of thiol-functionalization of magnetic graphene oxide and superparamagnetic Fe_3O_4@SiO_2 for Hg(II) removal from aqueous solution and petrochemical wastewater, *J. Taiwan Inst. Chem. Eng.*, 95, 78–93.

[28] Oluwasina, O.O., Ranu, S., Jonnalagadda, S.B., and Martincigh, B.S., 2021, Synthesis and characterization of graphene oxide under different conditions, and a preliminary study on its efficacy to adsorb Cu^{2+}, *Adv. Sci. Technol. Eng Syst. J.*, 6, 10–16.

[29] Langmuir, I., 1918, The adsorption of gases on plane surfaces of glass, mica and platinum, *J. Am. Chem. Soc.*, 40 (9), 1361–1403.

[30] Freundlich, H., 1906, Über die adsorption in lösungen, *Z. Phys. Chem.*, 57, 385–471.

[31] Sips, R., 1948, On the structure of a catalyst surface, *J. Chem. Phys.,* 16, 490–495.

[32] Temkin, M.I., and Pyzhev, V., 1940, Kinetics of ammonia synthesis on promoted iron catalyst, *Acta Physicochim. URSS*, 12, 327–356.

[33] Dubinin, M.M., 1947, The equation of the characteristic curve of activated charcoal, *Dokl. Akad. Nauk SSSR*, 55, 327–329.

[34] Redlich, O., and Peterson, D., 1959, A useful adsorption isotherm, *J. Phys. Chem.*, 63 (6), 1024.

[35] Yadav, A., Bagotia, N., Sharma, A.K., and Kumar, S., 2021, Simultaneous adsorptive removal of conventional and emerging contaminants in multi-component systems for wastewater remediation: A critical review, *Sci. Total Environ.*, 799, 149500.

[36] Ho, Y.S., 2003, Removal of copper ions from aqueous solution by tree fern, *Water Res.*, 37 (10), 2323–2330.

[37] Ho, Y.S., 2004, Comment on "Cadmium removal from aqueous solutions by chitin: Kinetic and equilibrium studies", *Water Res.*, 38 (12), 2962–2964.

[38] Somsesta, N., Sricharoenchaikul, V., and Aht-Ong, D., 2020, Adsorption removal of methylene blue onto activated carbon/cellulose biocomposite films: Equilibrium and kinetic studies, *Mater. Chem. Phys.*, 240, 122221–122231.

[39] Demirbas, E., Kobya, M., Senturk, E., and Ozkan, T., 2004, Adsorption kinetics for the removal of chromium(VI) from aqueous solutions on the activated carbons prepared from agricultural wastes, *Water SA*, 30, 533–539.

[40] Chien, S.H., and Clayton, W.R., 1980, Application of Elovich equation to the kinetics of phosphate release and sorption in soils, *Soil Sci. Soc. Am. J.*, 44 (2), 265–268.

[41] Ball, P.C., and Evans, R., 1989, Temperature dependence of gas adsorption on a mesoporous solid: Capillary criticality and hysteresis, *Langmuir*, 5 (3), 714–723.

[42] Wang, Y., Wei, X., Qi, Y., and Huang, H., 2021, Efficient removal of bisphenol-A from water and wastewater by Fe_2O_3-modified graphene oxide, *Chemosphere*, 263, 127563.

[43] Permadi, A., Fahmi, M.Z., Chen, J.K., Chang, J.Y., Cheng, C.Y., Wang, G.Q., and Ou, K.L., 2012, Preparation of poly(ethylene glycol) methacrylate coated $CuInS_2$/ZnS quantum dots and their use in cell staining, *RSC Adv.*, 2 (14), 6018–6022.

[44] Hu, Z.P., Gao, Z.M., Liu, X., and Yuan, Z.Y., 2018, High-surface-area activated red mud for efficient removal of methylene blue from wastewater, *Adsorpt. Sci. Technol.*, 36 (1-2), 62–79.

[45] Rao, C.V., Giri, A.S., Goud, V.V., and Golder, A.K., 2016, Studies on pH-dependent colour variation and decomposition mechanism of Brilliant Green dye in Fenton reaction, *Int. J. Ind. Chem.*, 7 (1), 71–80.

[46] Xu, H., Jia, W., Ren, S., and Wang, J., 2019, Magnetically responsive multi-wall carbon nanotubes as recyclable demulsifier for oil removal from crude oil-in-water emulsion with different pH levels, *Carbon*, 145, 229–239.

[47] Xu, H., Jia, W., Ren, S., and Wang, J., 2018, Novel and recyclable demulsifier of expanded perlite grafted by magnetic nanoparticles for oil separation from emulsified oil wastewaters, *Chem. Eng. J.*, 337, 10–18.

[48] Lin, C.C., and Lee, C.Y., 2020, Adsorption of ciprofloxacin in water using Fe_3O_4 nanoparticles formed at low temperature and high reactant concentrations in a rotating packed bed with co-precipitation, *Mater. Chem. Phys.*, 240, 122049.

[49] Shahnaz, T., Patra, C., Sharma, V., and Selvaraju, N., 2020, A comparative study of raw, acid-modified and EDTA-complexed *Acacia auriculiformis* biomass for the removal of hexavalent chromium, *Chem. Ecol.*, 36 (4), 360–381.

[50] Liu, J., Wang, N., Zhang, H., and Baeyens, J., 2019, Adsorption of Congo red dye on $Fe_xCo_{3-x}O_4$ nanoparticles, *J. Environ. Manage.*, 238, 473–483.

[51] Sitko, R., Turek, E., Zawisza, B., Malicka, E., Talik, E., Heimann, J., Gagor, A., Feist, B., and Wrzalik, R., 2013, Adsorption of divalent metal ions from aqueous solutions using graphene oxide, *Dalton Trans.*, 42 (16), 5682–5689.

[52] Eeshwarasinghe, D., Loganathan, P., Kalaruban, M., Sounthararajah, D.P., Kandasamy, J., and Vigneswaran, S., 2018, Removing polycyclic aromatic hydrocarbons from water using granular activated carbon: Kinetic and equilibrium adsorption studies, *Environ. Sci. Pollut. Res.*, 25 (14), 13511–13524.

[53] Travlou, N.A., Kyzas, G.Z., Lazaridis, N.K., and Deliyanni, E.A., 2013, Graphite oxide/chitosan composite for reactive dye removal, *Chem. Eng. J.*, 217, 256–265.

[54] Al-Asheh, S., Banat, F., Al-Omari, R., and Duvnjak, Z., 2000, Predictions of binary sorption isotherms for the sorption of heavy metals by pine bark using single isotherm data, *Chemosphere*, 41 (5), 659–665.

[55] Shirsath, S.R., Patil, A.P., Patil, R., Naik, J.B., Gogate, P.R., and Sonawane, S.H., 2013, Removal of brilliant green from wastewater using conventional and ultrasonically prepared poly(acrylic acid) hydrogel loaded with kaolin clay: A comparative study, *Ultrason. Sonochem.*, 20 (3), 914–923.

[56] Maebana, M.O., Mishra, S.B., Mamba, B.B., and Mishra, A.K., 2013, Study on the efficiency of ethylene vinyl acetate–fly ash composites for the uptake of phenols from synthetic waste water, *J. Appl. Polym. Sci.*, 128 (3), 2073–2080.

[57] El-Bindary, A.A., Hussien, M.A., Diab, M.A., and Eessa, A.M., 2014, Adsorption of Acid Yellow 99 by polyacrylonitrile/activated carbon composite: Kinetics, thermodynamics and isotherm studies, *J. Mol. Liq.*, 197, 236–242.

[58] Ooi, J., Lee, L.Y., Hiew, B.Y.Z., Thangalazhy-Gopakumar, S., Lim, S.S., and Gan, S., 2017, Assessment of fish scales waste as a low cost and eco-friendly adsorbent for removal of an azo dye: Equilibrium, kinetic and thermodynamic studies, *Bioresour. Technol.*, 245, 656–664.

[59] Ragab, A., Ahmed, I., and Bader, D., 2019, The removal of brilliant green dye from aqueous solution using nano hydroxyapatite/chitosan composite as a sorbent, *Molecules*, 24 (5), 847.

[60] Segun Esan, O., Nurudeen Abiola, O., Owoyomi, O., Olumuyiwa Aboluwoye, C., and Olubunmi Osundiya, M., 2014, Adsorption of brilliant green onto Luffa cylindrical sponge: Equilibrium, kinetics, and thermodynamic studies, *ISRN Phys. Chem.*, 2014, 743532.

[61] Giri, B.S., Gun, S., Pandey, S., Trivedi, A., Kapoor, R.T., Singh, R.P., Abdeldayem, O.M., Rene, E.R., Yadav, S., Chaturvedi, P., Sharma, N., and Singh, R.S., 2020, Reusability of brilliant green dye contaminated wastewater using corncob biochar and *Brevibacillus parabrevis*: Hybrid treatment and kinetic studies, *Bioengineered*, 11 (1), 743–758.

[62] Sukla Baidya, K., and Kumar, U., 2021, Adsorption of brilliant green dye from aqueous solution onto

chemically modified areca nut husk, *S. Afr. J. Chem. Eng.*, 35, 33–43.

[63] Tanyol, M., Kavak, N., and Torğut, G., 2019, Synthesis of poly(AN-co-VP)/zeolite composite and its application for the removal of brilliant green by adsorption process: Kinetics, isotherms, and experimental design, *Adv. Polym. Technol.*, 2019, 8482975.

[64] Doke, K.M., and Khan, E.M., 2013, Adsorption thermodynamics to clean up wastewater; Critical review, *Rev. Environ. Sci. Bio/Technol.*, 12 (1), 25–44.

[65] Aichour, A., and Zaghouane-Boudiaf, H., 2019, Highly brilliant green removal from wastewater by mesoporous adsorbents: Kinetics, thermodynamics and equilibrium isotherm studies, *Microchem. J.*, 146, 1255–1262.

[66] Mansour, R.A., El Shahawy, A., Attia, A., and Beheary, M.S., 2020, Brilliant green dye biosorption using activated carbon derived from guava tree wood, *Int. J. Chem. Eng.*, 2020, 8053828.

[67] Coşkun, Y.I., Aksuner, N., and Yanik, J., 2019, Sandpaper wastes as adsorbent for the removal of brilliant green and malachite green dye, *Acta Chim. Slov.*, 66 (2), 402–413.

[68] Kataria, N., and Garg, V.K., 2019, Application of EDTA modified Fe_3O_4/sawdust carbon nanocomposites to ameliorate methylene blue and brilliant green dye laden water, *Environ. Res.*, 172, 43–54.

[69] Thakur, S., Singh, S., and Pal, B., 2021, Superior adsorptive removal of brilliant green and phenol red dyes mixture by CaO nanoparticles extracted from egg shells, *J. Nanostruct. Chem.*, 12 (2), 207–221.

[70] Romzi, A.A., Lim, L.B.L., Chan, C.M., and Priyantha, N., 2020, Application of *Dimocarpus longan* ssp. *malesianus* leaves in the sequestration of toxic brilliant green dye, *Desalin. Water Treat.*, 189, 428–439.

[71] Zolgharnein, J., Bagtash, M., and Shariatmanesh, T., 2015, Simultaneous removal of binary mixture of brilliant green and crystal violet using derivative spectrophotometric determination, multivariate optimization and adsorption characterization of dyes on surfactant modified nano-γ-alumina, *Spectrochim. Acta, Part A*, 137, 1016–1028.

[72] Saif Ur Rehman, M., Kim, I., Rashid, N., Adeel Umer, M., Sajid, M., and Han, J.I., 2016, Adsorption of brilliant green dye on biochar prepared from lignocellulosic bioethanol plant waste, *Clean: Soil, Air, Water*, 44 (1), 55–62.

[73] Ur Rehman, M.S., Munir, M., Ashfaq, M, Rashid, N., Nazar, M., Danish, M., and Han, J.I., 2013, Adsorption of brilliant green dye from aqueous solution onto red clay, *Chem. Eng. J.*, 228, 54–62.

[74] Asadullah, M., Asaduzzaman, M., Kabir, M.S., Mostofa, M.G., and Miyazawa, T., 2010, Chemical and structural evaluations of activated carbon prepared from jute sticks for brilliant green dye removal from aqueous solution, *J. Hazard. Mater.*, 174 (1-3), 437–443.

[75] Mansour, R.A.E.G., Simeda, M.G., and Zaatout, A.A., 2021, Removal of brilliant green dye from synthetic wastewater under batch mode using chemically activated date pit carbon, *RSC Adv.*, 11, 14, 7851–7861.

[76] Li, Z., Hanafy, H., Zhang, L., Sellaoui, L., Netto, M.S., Oliveira, M.L., Seliem, M.K., Datto, G.L., Petriciolet, A.B., and Li, Q., 2020, Adsorption of Congo red and methylene blue dyes on an ashitaba waste and a walnut shell-based activated carbon from aqueous solutions: Experiments, characterization and physical interpretations, *Chem. Eng. J.*, 388, 124263.

[77] Lv, M., Yan, L., Liu, C., Su, C., Zhou, Q., Zhang, X., Lan, Y., Zheng, Y., Lai, L., Liu, X., and Ye, Z., 2018, Non-covalent functionalized graphene oxide (GO) adsorbent with an organic gelator for co-adsorption of dye, endocrine-disruptor, pharmaceutical and metal ion, *Chem. Eng. J.*, 349 (1), 791–799.

[78] Verma, A., Thakur, S., Mamba, G., Prateek, P., Gupta, R.K., Thakur, P., and Thakur, V.K., 2020, Graphite modified sodium alginate hydrogel composite for efficient removal of malachite green dye, *Int. J. Biol. Macromol.*, 148, 1130–1139.

[79] Wang, X., Zhang, Y., Shan, R., and Hu, H., 2020, Polydopamine interface encapsulating graphene

and immobilizing ultra-small, active Fe_3O_4 nanoparticles for organic dye adsorption, *Ceram. Int.*, 47 (3), 3219–3231.

[80] Wang, S., Wei, J., Lv, S., Guo, Z., and Jiang, F., 2013, Removal of organic dyes in environmental water onto magnetic-sulfonic graphene nanocomposite, *Clean: Soil, Air, Water*, 41 (10), 992–1001.

[81] Ighalo, J.O., Adeniyi, A.G., and Adelodun, A.A., 2021, Recent advances on the adsorption of herbicides and pesticides from polluted waters: Performance evaluation via physical attributes, *J. Ind. Eng. Chem.*, 93, 117–137.

[82] Raharjo, Y., Fahmi, Z., Wafiroh, W., Widati, A.A., Amanda, E.R., Ismail, A.F., Othman M.H.D., and Santoso, D., 2019, Incorporation of imprinted-zeolite to polyethersulfone/cellulose acetate membrane for creatinine removal in hemodialysis treatment, *Jurnal Teknologi*, 81 (3), 137–144.